Journal of Organometallic Chemistry 806 (2016) 22–32

Contents lists available at ScienceDirect

Journal of Organometallic Chemistry

journal homepage: www.elsevier.com/locate/jorganchem

Strained metal bonding environments in methylindium dithiolates and their reactivity as initiators for the ring-opening polymerization of cyclic esters

Glen G. Briand [a, *], Stefan A. Cairns [b], Andreas Decken [c], Courtney M. Dickie [a], Thomas I. Kostelnik [a], Michael P. Shaver [b]

[a] Department of Chemistry and Biochemistry, Mount Allison University, Sackville, New Brunswick E4L 1G8, Canada
[b] School of Chemistry, University of Edinburgh, David Brewster Road, Edinburgh, EH9 3FJ, United Kingdom
[c] Department of Chemistry, University of New Brunswick, Fredericton, New Brunswick E3B 6E2, Canada

ARTICLE INFO

Article history:
Received 20 November 2015
Received in revised form
12 January 2016
Accepted 13 January 2016
Available online 19 January 2016

Keywords:
Indium
Thiolate
X-ray diffraction
Catalysis
ROP
Cyclic esters

ABSTRACT

We have synthesized indium complexes containing a variety of metal bonding environments through use of polyfunctional dithiolate ligands and examined their reactivity as initiators for the ring-opening polymerization of L-lactide, rac-lactide, ε-caprolactone and β-butyrolactone. The facile reaction of Me3In with the corresponding polyfunctional dithiols in toluene, thf or diethyl ether resulted in the formation of [MeIn(SOOS)]2 (3), MeIn(SNNS) (4), [MeIn(ONS2)]3 (5), MeIn(NNS2) (6), MeIn(NNS2Pr) (7) and MeIn(pyrS)2 (8). The solid-state structures of 3 and 5 each show the corresponding ligand to be tridentate with an uncoordinated ligand O atom. Dimeric (3) and trimeric (5) structures result from short intermolecular In … S interactions. All structures show five coordinate indium centres in distorted trigonal bipyramidal bonding environments, but with various arrangements of donor atoms (eq/ax): SSC/OS (3,5), SNC/NS (4), SSN/NC (6), SSC/NS (7) and SSC/NN (8). DFT studies of model MeIn(SMe)2(NH3)2 systems show the bonding environments in 4 and 6 to be highly strained, while the axial In—Me bond of 6 shows the longest bond distance and lowest vibrational frequency. Compound 5 provided the best control of the polymerization of L-lactide and rac-lactide in THF at 70 °C, and a small heterotactic enrichment was observed for the latter. Compounds 3 and 4 provided the best control of the polymerization of β-BL in toluene at 70 °C in toluene, and compound 3 provided the best control of the polymerization of ε-CL in toluene at 70 °C. In all cases, polymerization rates were low. This work demonstrates a systematic approach to exploring the modification and reactivity of main group metal bonding motifs, which has resulted in identification of two novel "strained" bonding environments for indium.

1. Introduction

Over the past 20 years, interest in main-group element catalyzed ring opening polymerization (ROP) to obtain aliphatic polyesters has been steadily increasing due to applications in the pharmaceutical and commodity plastics industries [1–6], as has the prevalence of main group catalysis in small molecule chemistry [7]. Therefore, a primary focus of contemporary main group chemistry is the identification of reactive species for use as improved alternatives to traditional transition metal-based catalysts in chemical processes [8]. Such studies often explore novel bonding situations for main group elements where reactivity is manipulated through electronic inductive effects of ligands or modification of the element's bonding environment. The latter is intimately related to electronic structure as the most stable structures for covalently bonded species must adhere to VSEPR rules and valence bond models [9].

While aluminum compounds displayed both early and continued success in catalyzing the ring opening polymerization of *rac*-lactide, ε-caprolactone and many other monomers [10,11], exceptional catalysts have more recently been prepared by the heavier indium analogues. In fact, ligand-supported indium

* Corresponding author.
E-mail address: gbriand@mta.ca (G.G. Briand).

http://dx.doi.org/10.1016/j.jorganchem.2016.01.020
0022-328X/

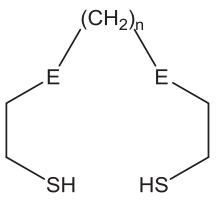

H_2(SOOS), E = O, n = 2
H_2(SNNS), E = NMe, n = 2
H_2(SNNSPr), E = NEt, n = 3

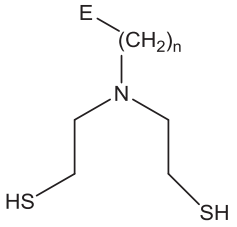

$H_2(ONS_2)$, E = OMe, n = 2
$H_2(NNS_2)$, E = NEt_2, n = 2
$H_2(NNS_2Pr)$, E = NEt_2, n = 3

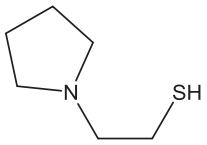

H(pyrS)

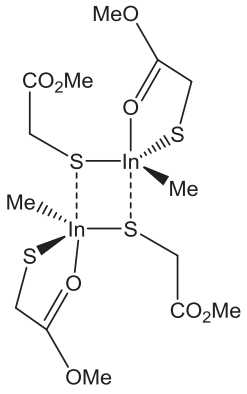

1

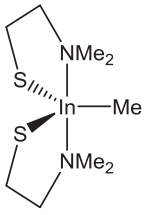

2

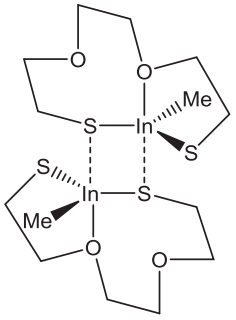

$[MeIn(SOOS)]_2$ (**3**)

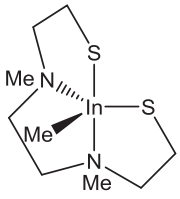

[MeIn(SNNS)] (**4**)

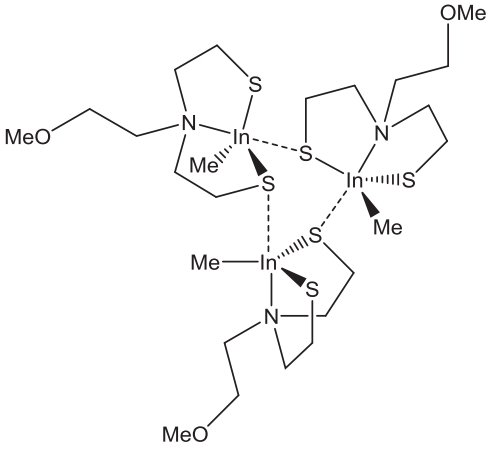

$[MeIn(ONS_2)]_3$ (**5**)

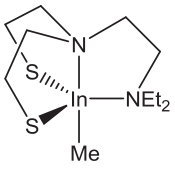

[MeIn(NNS_2)] (**6**)

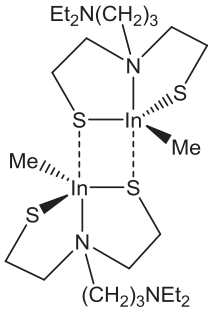

$[MeIn(NNS_2Pr)]_2$ (**7**)

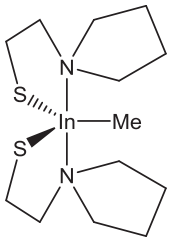

$[MeIn(pyrS)_2]$ (**8**)

catalysts are now some of the better ROP mediators for lactide [12–22], ε-caprolactone [19,23] and β-butyrolactone [19,24] polymerisations. There remains a dearth of systematic studies of ligand effects in this area, however, even though indium based catalysts are attractive due to their biocompatibility and moisture stability.

In light of this, we recently reported the synthesis of $[MeIn(SCH_2C(O)OMe)_2]_2$ (**1**) and $[MeIn(SCH_2CH_2NMe_2)_2]$ (**2**), and their ability to initiate the ROP of *rac*-lactide and ε-caprolactone [25]. The compounds incorporate bifunctional ester- or amino-thiolate ligands, and exhibit trigonal bipyramidal metal bonding environments with equatorial covalent bonds and axial dative bonds as predicted by valence bond theory for an sp^2 hybridized indium centre. To further explore the reactivity of the methylindium dithiolate system, we have prepared **3**–**7**. These compounds incorporate linear and tripodal polyfunctional amino/oxodithiolate ligands that constrain the positions of donor atoms in the coordination sphere and systematically alter the indium bonding environment. The induced reactivity of these compounds was probed through their ability to mediate the ROP reaction of L-lactide, *rac*-lactide, ε-caprolactone and β-butyrolactone. Further, we have prepared **8**, a more sterically inhibited analogue of **2**, with the potential to improve tacticity control in the ROP of *rac*-lactide.

2. Results and discussion

2.1. Synthesis and spectroscopic characterization

All compounds were prepared via the hydrocarbon elimination reaction between trimethylindium

and one (**3**–**7**) or two (**8**) equivalents of the corresponding (di) thiol. All reactions occurred rapidly at room temperature with evolution of methane gas. Reaction mixtures were stirred for 3 h and filtered to remove any precipitated product. Crystalline materials were isolated by slow evaporation, solvent layering, or cooling of reaction mixtures. Yields of **3**–**6** and **8** were moderate to good (69–83%). Compound **7** could not be isolated directly from the reaction mixture, and required removal of the reaction solvent under vacuum followed by extraction of the resulting gel with hexane. Slow evaporation of this solution afforded a low yield (21%) of crystalline product. An analogous reaction of $InMe_3$ and H_2(SNNSPr) in toluene or thf resulted in the formation an insoluble powder, while the 1:2 reaction of Me_3In with $iBu_2NCH_2CH_2SH$ in toluene gave an oil. The 1:2 reaction of Me_3In with $Bn_2NCH_2CH_2SH$ in toluene gave an insoluble product after layering of the reaction mixture with hexanes. These materials could not be definitively characterized and were not pursued further. The FT-Raman spectra of all compounds show a very strong resonance in the ~475-505 cm^{-1} range corresponding to the ν(In–C_{Me}) vibrational mode (vide infra). Strong and equal intensity vibrations at 480 and 505 cm^{-1} in crystalline samples of **4** isolated by cooling the reaction filtrate confirm the presence of both monomeric and dimeric structures, respectively, in the solid state. The reaction precipitate shows a weak signal at 480 cm^{-1} and a very strong signal at 505 cm^{-1}, indicating the presence of mainly dimeric species.

All compounds show signals at ~0 ppm in the ^1H NMR and −1 to −5 ppm in the $^{13}C\{^1H\}$ spectra corresponding to the In–*Me* group, as well as the expected ligand resonances. All compounds show a single set of sharp resonances for the corresponding dithiolate ligand, indicating monomeric species in the $CDCl_3$ solution at room temperature. Further, NMR spectra show that the ligands are symmetric in solution, indicating that the metal bonding environments observed in the solid state, i.e. those of **3** and **4**, are fluxional in solution at 23 °C.

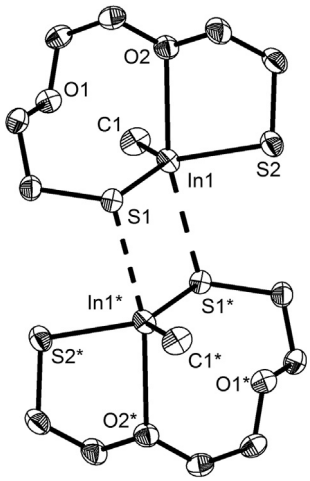

Fig. 1. X-ray structure of **3** (30% probability ellipsoids). Hydrogen atoms are not shown for clarity. Symmetry transformations used to generate equivalent atoms: (*) -x, -y + 1, -z + 2. Selected bond distances (Å) and angles (deg): In1–C1 = 2.149(2), In1–S1 = 2.4975(6), In1–S2 = 2.4483(6), In1–S1* = 2.8072(6), In1–O1 = 2.932(2), In1–O2 = 2.560(2), C1–In1–S1 = 127.31(7), C1–In1–S2 = 129.69(7), S1–In1–S2 = 102.95(2), O2–In1–S1* = 166.10(3).

2.2. X-ray crystal structures

Crystals suitable for X-ray crystallographic analysis were isolated by the slow evaporation at 23 °C (**3, 8**), solvent layering (**5**), or cooling of the reaction mixture (**4**, **6**). Crystals of **7** were isolated by extraction of the evaporated reaction mixture with hexanes followed by slow evaporation at 23 °C. Suitable refinement of the crystal structures of compounds **5** [26] and **7** [27] were not possible due to disorder. However, the metal bonding environment and oligomeric structures could be elucidated and are described below (see Supplementary data).

The structure of $[MeIn(SOOS)]_2$ (**3**) (Fig. 1) shows a dimer via intermolecular In1 … S1* interactions. One oxygen atom of the SOOS ligand is much more weakly coordinated to the indium centre [In1–O1 = 2.931(2) Å versus In1–O2 = 2.560(2) Å], but is within the sum of the van der Waals radii of indium and oxygen (3.45 Å) [28]. As expected, the In–S bond distance to the bridging sulfur atom [In1–S1 = 2.4975(6) Å] is significantly longer than that to the non-bridging sulfur atom [In1–S2 = 2.4483(6) Å]. Further, the In_2S_2

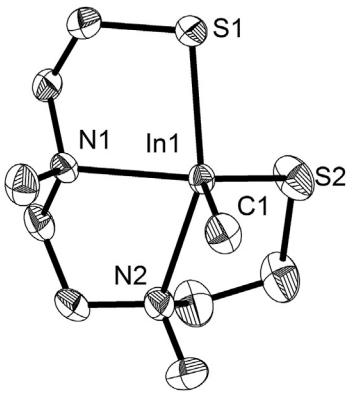

Fig. 2. X-ray structure of **4** (30% probability ellipsoids). Hydrogen atoms are not shown for clarity. Selected bond distances (Å) and angles (deg): In1–C1 = 2.156(5), In1–S1 = 2.523(3), In1–S2 = 2.455(2), In1–N1 = 2.348(4), In1–N2 = 2.515(4), C1–In1–S2 = 125.7(1), C1–In1–N1 = 109.0(2), N1–In1–S2 = 120.95(9), N2–In1–S1 = 149.67(9).

ring bond distance In1–S1* [2.8072(6) Å] is significantly longer than In1–S1. This is presumably a result of the trans influence of the ether oxygen atom (O2), and yields an asymmetric In_2S_2 core. If the long In1–O1 interaction is ignored, the indium centre is in a distorted trigonal bipyramidal bonding environment, with two sulfur atoms of a SOOS ligand and a methyl carbon atom in equatorial positions [C1–In1–S1 = 127.31(7)°, C1–In1–S2 = 129.69(7)°, S1–In1–S2 = 102.95(2)°], and an SOOS oxygen atom and a sulfur atom from a bridging SOOS ligand in axial positions [O2–In1–S1* = 166.10(3)°]. Overall, this dimeric structure resembles that of **1** [22]. If the In1–O1 interaction is considered, the geometry can be described as irregular or very distorted octahedral.

In contrast to **3**, the structure of MeIn(SNNS) (**4**) (Fig. 2) shows the compound to be a monomer in the solid-state. It exhibits one tetradentate SNNS ligand and a five coordinate S_2N_2C bonding environment for indium. The In1–S1 bond distance [2.523(3) Å] is significantly longer than In1–S2 [2.455(2) Å], while In1–N2 [2.515(4) Å] is significantly longer than In–N1 [2.348(4) Å]. The In1–C1 [2.156(5) Å] bond distance is similar to those observed in **1**–**3**. The bond distances and angles suggest a distorted trigonal bipyramidal geometry at indium, with the one thiolate sulfur atom, an amine nitrogen atom, and the methyl carbon atom in equatorial positions [C1–In1–S2 = 125.7(1)°, C1–In1–N1 = 109.0(2)°, N1–In1–S2 = 120.95(9)°], and an amine nitrogen atom and a thiolate sulfur atom in axial positions [N2–In1–S1 = 149.67(9)°].

The preliminary structure of [MeIn(ONS_2)]$_3$ (**5**) shows a trimer via intermolecular In … S interactions and yields an In_3S_3 core (see structural drawing of **5** and Supplementary data for geometry optimized structure). All three unique indium centres show similar bonding environments. The ONS_2 ligand is bonded in a tridentate *N,S,S* manner with the ether oxygen atom not being coordinated to the metal centre. The bond distances and angles suggest a distorted trigonal bipyramidal geometry at indium, with the two thiolate sulfur atom and the methyl carbon atom in equatorial positions and an amine nitrogen atom and a thiolate sulfur atom in axial positions. Further, the In_3S_3 ring bond distances are significantly different, with that trans to the amine nitrogen atom being larger by ~0.2 Å.

Like **4**, the structure of MeIn(NNS_2) (**6**) (Fig. 3) shows the compound to be a monomer in the solid-state. It exhibits one tetradentate NNS_2 ligand and a five coordinate S_2N_2C bonding environment for indium. The In1–S1 [2.4857(9) Å] and In1–S2 [2.4615(8) Å] bond distances differ only slightly, while In1–N1 [2.550(2) Å] is significantly longer than In–N2 [2.389(2) Å]. The In1–C1 [2.193(3) Å] bond distance is longer than those observed in **3** and **5**. The bond distances and angles suggest a distorted trigonal bipyramidal geometry at indium, with two thiolate sulfur atoms

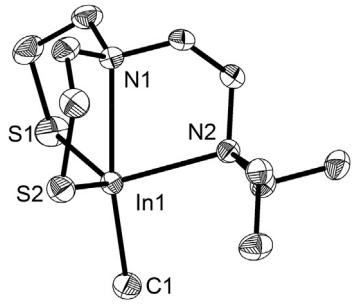

Fig. 3. X-ray structure of **6** (30% probability ellipsoids). Hydrogen atoms are not shown for clarity. Selected bond distances (Å) and angles (deg): In1–C1 = 2.193(3), In1–S1 = 2.4857(9), In1–S2 = 2.4615(8), In1–N1 = 2.550(2), In1– N2 = 2.389(2), N2–In1–S1 = 114.50(5), N2–In1–S2 = 108.82(5), S1–In1–S2 = 122.78(3), N1–In1–C1 = 169.9(1).

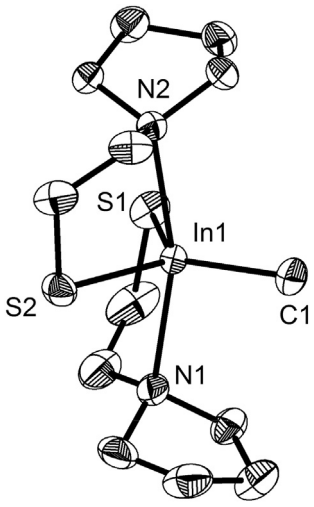

Fig. 4. X-ray structure of **8** (30% probability ellipsoids). Hydrogen atoms are not shown for clarity. Selected bond distances (Å) and angles (deg): In1–C1 = 2.165(2), In1–S1 = 2.4518(7), In1–S2 = 2.4717(7), In1–N1 = 2.481(2), In1– N2 = 2.468(2), S1–In1–S2 = 120.05(3), S1–In1–C1 = 123.31(7), S2–In1–C1 = 116.64(7), N1–In1–N2 = 163.14(5).

and an amine nitrogen atom in equatorial positions [N2–In1–S1 = 114.50(5)°, N2–In1–S2 = 108.82(5)°, S1–In1–S2 = 122.78(3)°], and an amine nitrogen atom and the methyl carbon atom in axial positions [N1–In1–C1 = 169.9(1)°].

The preliminary structure of [MeIn(NNS_2Pr)]$_3$ (**7**) shows a dimer via intermolecular In … S interactions and yields an In_2S_2 core (see structural drawing of **7** and Supplementary data for geometry optimized structure). The unique indium centres show similar bonding environments. The NNS_2 ligand is bonded in a tridentate *N,S,S* manner with the diethylamino-nitrogen atom not being coordinated to the metal centre. The bond distances and angles suggest a distorted trigonal bipyramidal geometry at indium, with the two thiolate sulfur atom and the methyl carbon atom in equatorial positions and an amine nitrogen atom and a thiolate sulfur atom in axial positions. Further, the In_2S_2 ring bond distances are significantly different, with that trans to the amine nitrogen atom being larger. Overall, the metal bonding environment and ligand bonding mode is similar to that of **5**, with **7** exhibiting a dimeric rather than a trimeric structure.

The structure of MeIn($pyrS$)$_2$ (**8**) (Fig. 4) shows the compound to be monomeric in the solid-state. It exhibits two chelating $-SCH_2CH_2N(CH_2)_4$ ligands and a five coordinate S_2N_2C bonding environment for indium [In1–S1 = 2.4518(7) Å; In1–S2 = 2.4717(7) Å; In1–C1 = 2.165(2) Å; In–N1 = 2.481(2) Å; In1–N2 = 2.468(2) Å]. Bond angles suggest a distorted trigonal bipyramidal geometry at indium, with the two thiolate sulfur atoms and the methyl carbon atom in equatorial positions [C1–In1–S1 = 123.31(7)°,

Table 1
The sum of equatorial bond angles and the axial bond angle for trigonal bipyramidal compounds **1**–**8**.

	Σ eq-In-eq	ax-In-ax
1	358.4(3)	166.45(7)
2	359.9(1)	163.57(5)
3	360.0(2)	168.67(5)
4	355.7(4)	149.67(9)
5	359.7(6)	160.8(1)
6	344.3(2)	169.9(1)
7	359.8(1)	147.08(3)
8	360.0(1)	163.14(5)

C1–In1–S2 = 116.64(7)°, S1–In1–S = 120.05(3)°], and the amine nitrogen atoms in axial positions [N1–In1–N2 = 163.14(5)°]. The structure of **8** is similar to that of **2**, with the most significant metrical differences being the larger In–N bond distances in **8** [In1–N1 = 2.481(2) and In1–N2 = 2.468(2) Å] versus **2** [2.419(2) and 2.430(2) Å]. This is presumably a result of the increased steric bulk of the $-N(CH_2)_4$ rings in **8** versus the $-NMe_2$ groups in **2**.

The indium bonding environments of **1**–**8** may be described as five coordinate distorted trigonal bipyramidal (Table 1). However, the structures of **4** and **6** contrast that of **1**, **2** [22], **3**, **5**, **7** and **8**, other bicyclic $XIn(SCH_2CH_2NMe_2)_2$ [X = Cl, I, 4-MeC_6H_4S, 4-$MeOC_6H_4S$] compounds [29], and bis-amine adducts of indium trithiolates [e.g. $In(SPh)_3(py)_2$ and $In(SEt)_3(dmap)_2$] [30]. The latter possess covalent bonding interactions with anionic groups (i.e. thiolate, methyl or halide) in equatorial positions and dative bonding interactions with Lewis-base donor atoms (i.e. amine nitrogen, carbonyl/ether oxygen or bridging thiolate sulfur) in axial positions. Compound **4** shows equatorial bonding interactions with a thiolate sulfur, a methyl carbon and an amine nitrogen, and the axial interactions of an amine nitrogen and a thiolate sulfur atom. Compound **6** shows equatorial bonding interactions with two thiolate sulfur atoms and an amine nitrogen, and the axial interactions of an amine nitrogen and a methyl carbon. These indium bonding environments are strained with respect to the expected valence bond model for an sp^2 hybridized indium centre. To probe this further, we have performed computational studies to determine the relative stabilities of the various observed bonding environments at indium.

2.3. DFT computational studies

DFT calculations were performed to rationalize the observed structures and probe bonding at indium in **3**–**8**. Structural representations and parameter for the geometry-optimized structures are given in the Supplementary data and very similar to those of the corresponding compounds in the solid-state. Et_2N- groups were replaced with Me_2N- groups in $[MeIn(NNS_2)]_n$ and $[Me(NNS_2Pr)]_n$ to minimize computing time.

In order to gauge the relative stabilities of the observed N_2S_2C bonding environments in **2**,**4**,**6** and **8**, $InC_{Me}NNSS$ frozen atom optimizations were performed for $MeIn(SMe)_2(NH_3)_2$ using the metal bonding distances and angles in **2**, **4**, **6** and **8**. X-ray crystal structures, and their corresponding calculated structures with relative energies versus geometry optimized $MeIn(SMe)_2(NMe_3)_2$, are given in Fig. 5. The calculated energies show that the tethering of the amine nitrogen atoms to each of the sulfur atoms via a $-CH_2CH_2-$ linkage in **2** and **8** causes a minimal distortion of the preferred SSC/NN (eq/ax) indium bonding environment and a slightly higher energy. However, the tethering of the nitrogen and sulfur atoms in (SNNS) and (NNS_2) provides significant distortion versus the optimized indium bonding environment, with much higher energies (+44 and + 42 kJ mol^{-1}, respectively). This suggests a strained bonding environment and potentially greater reactivity for **4** and **6** versus **2** and **8**.

DFT calculations were also performed to provide insight into the preference for the observed monomeric (m), dimeric (d) and trimeric (t) solid-state structures. The energies associated with the dimerization and trimerization may be calculated using Eqs. (1) and (2), respectively.

$$2\ MeIn(SR')_2 \rightarrow [MeIn(SR')_2]_2 \quad \Delta E = E_d - 2E_m \tag{1}$$

$$3\ MeIn(SR')_2 \rightarrow [MeIn(SR')_2]_3 \quad \Delta E = E_t - 3E_m \tag{2}$$

The corresponding data are given in Table 2.

The negative ($E_d - 2E_m$) values calculated for $[MeIn(SOOS)]_n$ and $[Me(NNS_2Pr)]_n$ (−40 and −64 kJ mol^{-1}, respectively) indicate that dimerization is thermodynamically favourable in the gas

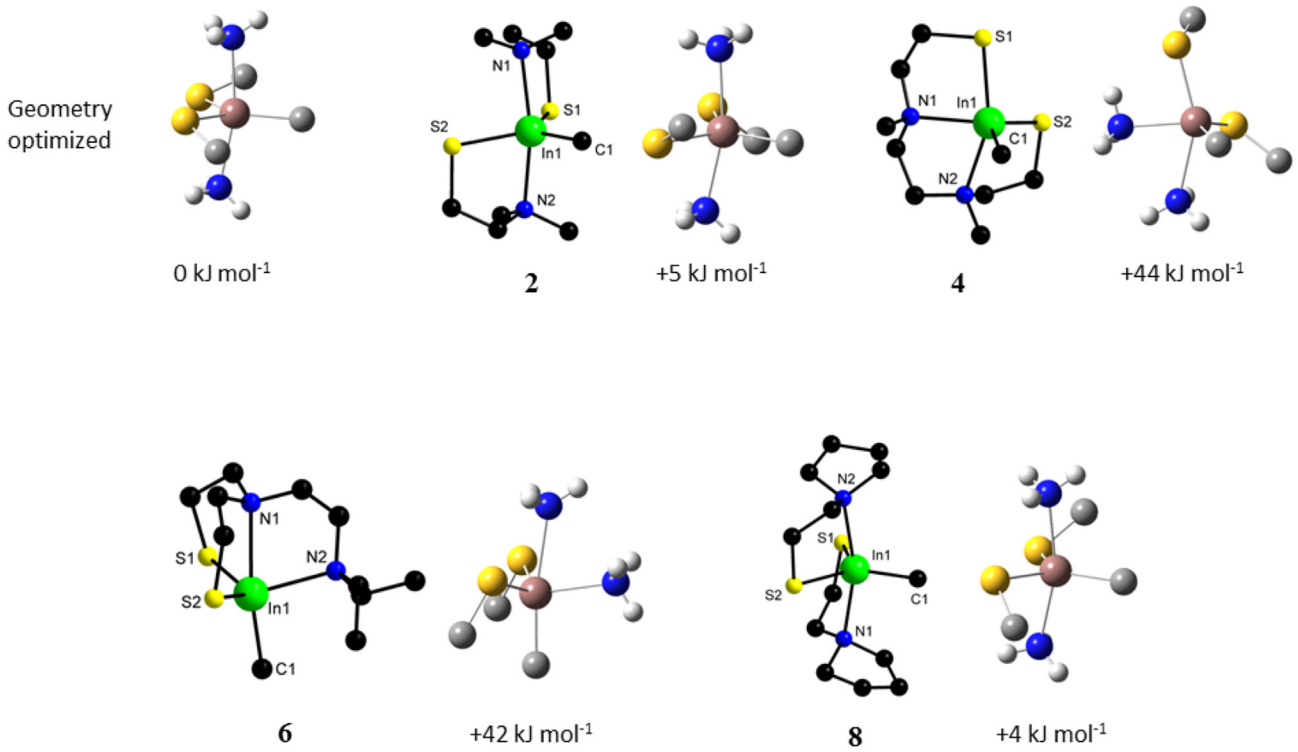

Fig. 5. Geometry optimized structures and calculated relative energies (E) of $(MeS)_2InMe(NH_3)_2$ for indium bonding environments **2**, **4**, **6** and **8**. Methyl hydrogen atoms are not shown for clarity.

Table 2
Calculated energies for geometry optimized monomeric (E_m), dimeric (E_d) and trimeric (E_t) MeIn(SR′)$_2$ species (kJ mol^{-1}).

	E_m (n = 1)	E_d (n = 2)	E_t (n = 3)	$E_d - 2E_m$	$E_t - 3E_m$
$[MeIn(SOOS)]_n$	−3214462	−6428965		−40	
$[Me(SNNS)]_n$	−3316351	−6632723		−20	
$[Me(ONS_2)]_n$	−3265399	−6530832	−9796252	−35 (−18)[a]	−56 (−19)[b]
$[MeIn(NNS_2)]_n$	−3316359	−6632721		+3	
$[Me(NNS_2Pr)]_n$	−3419475	−6839015		−64	
$[MeIn(pyrS)_2]_n$	−3725826	−7451601		+51	
$[MeIn(SNS)]_n$	−2861684	−5723445	−8585169	−78 (−39)[a]	−119 (−40)[b]

[a] $(E_d - 2E_m)/2$.
[b] $(E_t - 3E_m)/3$.

phase. Conversely, $[MeIn(NNS_2)]_2$ and $[MeIn(pyrS)_2]_2$ show positive values (+3 and + 51 kJ mol^{-1}, respectively) indicating that the monomeric structure is thermodynamically favourable in the gas phase. Finally, the negative ($E_t - 3E_m$) value calculated for $[MeIn(ONS_2)]_n$ (−56 kJ mol^{-1}) indicates that trimerization is thermodynamically favourable in the gas phase. These results are in accordance with the observed dimeric (**3**, **7**) and monomeric (**6**, **8**) solid-state structures, and suggest that the observed structures are not a result of packing forces. In contrast, a negative energy (−20 kJ mol^{-1}) was calculated for the formation of dimeric $[MeIn(SNNS)]_2$ while a monomeric structure was confirmed for **4** by X-ray crystallography. However, both monomeric and dimeric species are observed in the FT-Raman spectra of **4**, with the latter being predominant in the reaction precipitate (vide supra).

The electronic energy of $[MeIn(ONS_2)]_2$ was also calculated and shows a negative energy of dimerization (−35 kJ mol^{-1}). The electronic energies calculated for the dimerization and trimerization of $[Me(ONS_2)]_n$ (n = 2, 3) may be divided by n $[(E_d - 2E_m)/2$ and $[(E_t - 3E_m)/3]$ to give per monomer stabilization energy values, and may be compared directly. The calculated values are −18 kJ mol^{-1} for $[Me(ONS_2)]_2$ and −19 kJ mol^{-1} for $[Me(ONS_2)]_3$, supporting a small energy preference for the trimeric structure.

Comparison of the ($E_d - 2E_m$) values for $[MeIn(SOOS)]_n$ (−40 kJ mol^{-1}) and $[Me(SNNS)]_n$ (−20 kJ mol^{-1}) shows that the dimerization of the former is much more favorable. This is presumably a result of the weaker donor ability of the ligand oxygen versus nitrogen atoms, yielding a more Lewis acid center and more favorable intermolecular In … S contacts. Similarly, comparison of the analogous values for $[MeIn(ONS_2)]_n$ (−35 kJ mol^{-1}) and $[Me(NNS_2)]_n$ (+3 kJ mol^{-1}) also suggest a weaker In-E interaction for the oxygen versus nitrogen atom of the pendant $-CH_2CH_2E$ (E = OMe, NMe_2) group. The corresponding value for $[Me(NNS_2Pr)]_n$ (−64 kJ mol^{-1}) shows that replacing a ligand $-CH_2CH_2NMe_2$ group with a $-CH_2CH_2CH_2NMe_2$ group results in a weaker In–N interaction, which is also weaker than the In–O dative bonding interaction observed in $[MeIn(ONS_2)]_n$.

Table 3
In–C_{Me} bond distances and [ν(In–C_{Me})] FT-Raman stretching frequencies for **1**–**8** [experimental (calculated)].

	Bonding environment (eq/ax)[a]	d(In–C_{Me}) (Å)	ν(In–C_{Me}) (cm^{-1})
1	SSC/OS*	2.133(4) (2.15)	518 (510)
2	SSC/NN	2.177(2) (2.17)	484 (490)
3	SSC/OOS*	2.149(2) (2.14)	506 (510)
4	SNC/NS	2.156(5) (2.16)	480 (495)
5	SSC/NS*	2.147(8) (2.16)	497 (493)
6	SSN/CN	2.193(3) (2.18)	477 (483)
7	SSC/NS*	2.151(9) (2.15)	498 (505)
8	SSC/NN	2.165(2) (2.17)	491(490)

[a] S* indicates an intermolecular In … S bond.

2.4. Analysis of the In–C_{Me} bonding interaction

The strength of the In–C_{Me} bond is important in these compounds as this is the active site for catalytic activity in ROP studies. This bonding interaction may be probed through use of X-ray crystallography and FT-Raman data (Table 3). The data show that compounds containing intermolecular In … S bonds (**1**, **3**, **5** and **7**), i.e. dimeric and trimeric compounds, possess the shortest In–C bonds [2.133(4)-2.151(9) Å] and highest frequency resonances (497-518 cm^{-1}). This is presumably a result of the poor donor ability of the dithiolate ligand. Of the monomeric compounds, **4** exhibits a comparable In–C bond distance [2.156(5) Å] and a lower vibrational frequency [480 cm^{-1}] compared to the dimeric and trimeric structures. The favourable SSC/NN bonding environments (**2**, **8**) possesses both longer In–C bond distances [2.177(2) and 2.165(2) Å] and lower vibrational frequencies (484 and 491 cm^{-1}), as a result of the more efficient axial donor ability of the amine groups. The longest In–C bond distance [2.193(3) Å] and lowest vibrational frequency (477 cm^{-1}) is observed for the SSN/CN bonding environment (**6**), which has an axial methyl group that is nearly trans to an amine nitrogen atom.

2.5. Reaction of **3**–**6**, and **8** as initiators for the ROP of cyclic esters

Compounds **3**–**6** and **8** were screened as initiators for the ROP of cyclic esters. Initially, the polymerization of L-lactide in toluene at 110 °C was carried out using complexes **3**, **4**, and **8** (Table 4, entries 1–3). After 24 h each polymerization had reached >92% conversion. Compounds **4** and **8** produced polymers with low molecular weights compared to theoretical calculated values, the molecular weight distributions were not well controlled with dispersities of 1.47 and 1.45, respectively. As these polymerizations were carried out at elevated temperatures, an increased rate in competing transesterification reactions and low polymer molecular weights are expected. This is most evident for complex **3**, where the molecular weight of PLLA was less than half that of its theoretical value and the dispersity was very high at 2.52. These polymerization reactions were repeated at 85 °C (Table 4, entries 4, 5 and 6). Similar results were observed for compounds **4** and **8**, while polymerizations with compound **3** showed slightly better control of molecular weight and dispersity. Complexes **5** and **6** were capable of efficiently polymerizing L-lactide in THF at 70 °C, reaching 79% and 65% conversion, respectively, after 5 h (Table 4, entries 7 and 8). They also showed excellent control, producing polymers with molecular weights similar to theoretical values and dispersities (Đs) of 1.01 and 1.03 for compounds **5** and **6**, respectively.

The polymerization of *rac*-lactide in toluene at 110 °C was carried out using **3**, **4**, and **8** (Table 5, entries 1–3). Overall, similar results to those of the L-lactide reactions were obtained. After 24 h, the polymerizations had reached >97% conversion, molecular weights were low, and Đs were high (1.68, 1.55 and 1.64 for **3**, **4** and

Table 4
Ring opening polymerization of L-lactide using **3**–**6** and **8**.

Entry	Compound	Solvent	Temp./°C	Time/h	% conv.[a]	$M_{n,th}$[b]	M_n[c]	Đ[c]
1	**3**	Toluene	110	24	92	13356	5854	2.52
2	**4**	Toluene	110	24	98	14220	11553	1.47
3	**8**	Toluene	110	24	94	13644	10131	1.45
4	**3**	Toluene	85	24	99	14364	10799	1.61
5	**4**	Toluene	85	24	99	14364	10052	1.55
6	**8**	Toluene	85	24	96	13932	9755	1.61
7	**5**	THF	70	5	79	11380	11220	1.01
8	**6**	THF	70	5	65	9470	9820	1.03

Monomer:Complex:BnOH 100:1:1. Monomer concentration = 1 M.
[a] Monomer conversion (%) determined by ^{1}H NMR spectroscopy of crude sample.
[b] $M_{n,th}$ = ([M]/[BnOH]) × MW(monomer) × (% conv.) + MW (end group).
[c] Determined by gel permeation chromatography. Đ = dispersity = M_w/M_n.

Table 5
Ring opening polymerization of rac-lactide with **3**–**6** and **8**.

Entry	Compound	Solvent	Temp/°C.	Time/h	% conv.[a]	$M_{n,th}$[b]	M_n[c]	Đ[c]	P_r[d]
1	**3**	Toluene	110	24	97	14076	3740	1.68	/
2	**4**	Toluene	110	24	99	14364	8370	1.55	/
3	**8**	Toluene	110	24	98	14220	7210	1.64	/
4	**5**	THF	70	5	13	1980	/	/	/
5	**5**	THF	70	20	90	13068	11390	1.06	0.63
6	**6**	THF	70	5	64	9324	5920	1.01	0.68
7	**3**	bulk	120	0.5	99	3330	6300	1.89	/
8	**4**	bulk	120	0.5	84	8230	12580	1.53	/
9	**5**	bulk	120	0.5	99	8390	11330	1.35	/
10	**6**	bulk	120	0.5	97	14470	44800	3.12	/
11	**8**	bulk	120	0.5	99	16050	39900	2.49	/

Monomer:Complex:BnOH 100:1:1. Monomer concentration = 1 M.
[a] Monomer conversion (%) determined by ^{1}H NMR spectroscopy of crude sample.
[b] $M_{n,th}$ = ([M]/[BnOH]) × MW(monomer) × (% conv.) + MW (end group).
[c] Determined by gel permeation chromatography. Đ = dispersity = M_w/M_n.
[d] Pr is the probability of a racemic insertion of monomer units.

Table 6
Ring opening polymerization of β-butyrolactone using 3–6 and 8.

Entry	Compound	Solvent	Temp./°C	Time/h	% conv.[a]	$M_{n,th}$[b]	M_n[c]	Đ[c]
1	**3**	Toluene	70	96	95	8278	8360	1.17
2	**4**	Toluene	70	96	79	6902	7100	1.12
3	**5**	THF	70	96	98	8536	7670	1.15
4	**6**	THF	70	96	56	4924	2890	1.33
5	**8**	Toluene	70	96	5	538	490	1.17

Monomer:Complex:BnOH 100:1:1. Monomer concentration = 1 M.
[a] Monomer conversion (%) determined by ^{1}H NMR spectroscopy of crude sample.
[b] $M_{n,th}$ = [M]/[BnOH]) × MW(monomer) × (% conv.) + MW (end group).
[c] Determined by gel permeation chromatography. Đ = dispersity = M_w/M_n.

8, respectively). As for L-lactide, a high level of control was observed for the polymerization of *rac*-lactide with compounds **5** and **6** in THF at 70 °C (Table 5, entries 4–6). A 90% conversion was observed after 20 h for compound **5** and the polymer molecular weight was similar to theoretical values with a Đ of 1.06. However, it was found that reaction times were longer for the *rac*-lactide mixture than L-lactide alone (Table 4, entry 7), with a 13% conversion of *rac*-lactide versus a 79% of L-lactide after 5 h under the same conditions. This is potentially due to a lower polymerization rate for D-lactide in comparison to L-lactide. A 64% conversion was observed after 5 h for compound **6**. Although the molecular weight distribution was narrow with a Đ of 1.01, the PDLLA molecular weight was significantly lower than the theoretical value. A small level of heterotactic enrichment was observed in each case, with P_r values of 0.63 and 0.68 for polymerizations with compounds **5** and **6**, respectively (Figures S1 and S2). The best performance for our first generation In catalysts was the bulk ROP of *rac*-LA at 120 °C [24]. Polymerizations of *rac*-LA were also completed in bulk, showing extremely poor polymerization control. The high concentrations under these conditions do lead to rapid polymerizations; **3**–**6** and **8** each promote >84% monomer conversion in 30 min (Table 5, entries 7–11). Unfortunately, these forcing conditions also promote competing transesterification and very broad Đs.

Compounds **3**–**6** and **8** were tested for the polymerization of β-butyrolactone (β-BL) at 70 °C (Table 6). Reactions with compounds **3** and **5** reached high conversions of 95% and 98% after 96 h, respectively. Compounds **4** and **6** were less reactive, reaching 79% and 56% after 96 h, respectively. Complexes **3**, **4** and **5** displayed good control of the polymerization reaction, giving narrow Đs (<1.17) and experimental molecular weights similar to theoretical values. Compound **6** gave poor control of the reaction, yielding low molecular weight poly(3-hydroxybutyrate) and Đ = 1.33. Compound **8** did not polymerize β-BL under these conditions regardless of reaction time.

Table 7
Ring opening polymerization of ε-caprolactone using 3–6 and 8.

Entry	Compound	Solvent	Temp./°C	Time/h	% conv.[a]	$M_{n,th}$[b]	M_n[c]	Đ[c]
1	**3**	Tol	70	1	94	10824	8950	1.14
2	**4**	Tol	70	15	98	11280	10760	1.30
3	**5**	THF	70	24	86	9912	11490	1.28
4	**6**	THF	70	24	24	2844	2200	1.26
5	**8**	Tol	70	24	15	1818	/	/

Monomer:Complex:BnOH 100:1:1. Monomer concentration = 1 M.
[a] Monomer conversion (%) determined by ^{1}H NMR spectroscopy of crude sample.
[b] $M_{n,th}$ = ([M]/[BnOH]) × MW(monomer) × (% conv.) + MW (end group).
[c] Determined by gel permeation chromatography. Đ = dispersity = M_w/M_n.

Finally, compounds **3**–**6** and **8** were screened for the polymerization of ε-caprolactone. Compound **3** displayed the highest activity, polymerizing 100 equivalents of ε-CL to 94% conversion in toluene after 1 h at 70 °C, and the best control of the reaction, with a dispersity of 1.14 (Table 7, entry 1). Compound **4** required 15 h to achieve a similar conversion but also showed good control, producing polymers with molecular weights very similar to theoretical values and a narrow MW dispersity (1.30; Table 7, entry 2). After 24 h, compounds **5** and **6** gave conversions of 86 and 24%, respectively (Table 7, entries 3 and 4). Molecular weights were higher than theoretical values for polymerizations with compound **5**, which suggesting poor initiation, while those for the reaction with compound **6** were low. Đs were moderately high in both cases. Compound **8** again was the least active, reaching only 15% conversion after 24 h (Table 7, entry 5).

Overall, compound **5** provided the best control of the polymerization of L-lactide and *rac*-lactide in THF at 70 °C, with molecular weights similar to theoretical values and very narrow Đs. However, conversion rates were low for all catalysts. Interestingly, a modest heterotactic enrichment was observed. Contrastingly, compounds **3** and **4** provided the best control of the polymerization of β-BL in toluene at 70 °C in toluene, though conversion rates were low for all compounds tested. Compound **3** provided the best control of the polymerization of ε-caprolactone in toluene at 70 °C, with a reasonably high conversion, a molecular weight similar to the theoretical value, and a narrow Đ. The compounds with the most strained S_2N_2C bonding environments, i.e. compounds **4** and **6** (vide supra), appear to exhibit an increased reactivity over compound **8** toward β-BL and ε-CL, but similar reactivities toward L-lactide and *rac*-lactide. The increased steric bulk in compound **8** versus **2** does not yield a lower reactivity of the compound toward *rac*-lactide [24]. However, molecular weights are much lower as compared to theoretical values and Đs are much broader.

3. Conclusions

The hydrocarbon elimination reaction of trimethylindium and polyfunctional dithiols is a high yield route to cyclic indium dithiolate complexes. The ligand architecture and constraints imposed by the ligand backbone result in distorted and strained trigonal bipyramidal bonding environments for indium in the solid state. Most notable are those of **4** and **6** that feature thiolate sulfur and methyl carbon atoms in axial positions, respectively. This bonding mode differs from the typical valence bond description which predicts equatorial covalent bonds and axial dative interactions for sp^2 hybridized indium. Compounds **3** and **5** possess dimeric structures via intermolecular In … S bonding as a result of the poor donor ability of the secondary ether oxygen functionality versus amine functionality, while lengthening of the hydrocarbon backbone to the terminal amine group in **7** (NNS_2Pr) versus **6** (NNS_2) yields a less favourable In–N interaction and a preferred formation of an In … S interaction. NMR data suggests that all compounds are monomeric and dynamic behavior for the compounds in solution. ROP studies suggest that the dithiolate ligand design affects reactivity as those compounds containing the linear motif, i.e. SOOS (**3**) and SNNS (**4**), showed the highest activity and best control toward β-BL and ε-caprolactone, while compounds containing the tripodal motif, i.e. ONS_2 (**5**) and NNS_2 (**6**) showed the highest activity and best control toward L-lactide and *rac*-lactide. Further, the presence of weaker O versus N ligand donor atoms affords more reactive compounds (**3** and **5**). This is likely due to an increased ligand lability and Lewis acidity of the indium centre. The S_2N_2C compounds with the most strained bonding environments exhibit a higher reactivity toward some substrates, but the effect is not general. Increasing steric bulk in **8** versus **2** did not have the expected effect of increasing stereospecificity in the polymerization of *rac*-lactide, but instead led to lower activity and inferior control of the reaction. These observations will inform the design of the next generation of methylindium thiolate catalysts toward selective ROP catalysis.

4. Experimental

4.1. General considerations

Solution ^{1}H and $^{13}C\{^1H\}$ spectra were recorded at 23 °C on either a JEOL GMX 270 MHz + spectrometer (270 and 67.9 MHz, respectively), or a Varian Mercury 200 MHz + spectrometer (200 and 50 MHz, respectively), and chemical shifts are calibrated to the residual solvent signal. ATR FT-IR spectra were recorded on a Thermo Nicolet iS5 FT-IR spectrometer in the range of 4000–400 cm^{-1}. FT-Raman spectra were recorded on a Thermo Nicolet NXR 9600 Series FT-Raman spectrometer in the range 3900–70 cm^{-1}. Melting points were recorded on an Electrothermal MEL-TEMP melting point apparatus and are uncorrected. Elemental analyses were performed by Laboratoire d'analyse élémentaire, Université de Montréal, Montreal, Canada or Canadian Microanalytical Services, Delta, British Columbia, Canada. Gel permeation chromatography (GPC) was carried out in THF at a flow rate of 1 mL min−1 at 35 °C on a Malvern Instruments Viscotek 270 GPC Max triple detection system with 2 × mixed bed styrene/DVB columns (300 × 7.5 mm). dn/dc values of 0.051 for poly(lactide) [31], 0.065 poly(hydroxybutyrate) [32], 0.079 for poly(caprolactone) [33] were used to calculate molecular weights. Polymerizations were conducted under inert atmosphere using an MBraun LABmaster sp glovebox equipped with a −35 °C freezer, [O_2] and [H_2O] analyzers and a built-in Siemens Simantic Touch Panel.

2,2′-(Ethylenedioxy)diethanethiol 95%, *N,N*′-dimethylethylenediamine 85%, 2-methoxyethylamine 95%, *N,N*-diethylethylenediamine 99%, *N,N*′-diethyl-1,3-propanediamine 97%, 3-(diethylamino)propylamine >99%, dibenzylamine 97%, pyrrolidine 99%, and ethylene sulfide 98% were used as received from

Sigma–Aldrich. Trimethylindium was used as received from Strem. H_2(SNNS), H_2(SNNSPr) [34], H_2(ONS_2), H_2(NNS_2Pr) [35], H_2(NNS_2) [36], were prepared according to literature methods. H(pyrS) was prepared from the reaction of the corresponding amine with ethylene sulfide in toluene at 100 °C for 18 h. The solvent was removed and the residual liquid fractionally distilled under reduced pressure to give the desired product. D,L-lactide and L-lactide were purchased from Purac and were purified 3 × vacuum sublimations prior to polymerisation. ε-Caprolactone and benzyl alcohol were obtained from Sigma–Aldrich, dried over calcium hydride and distilled under inert atmosphere prior to use. Toluene, tetrahydrofuran (thf) and hexanes were dried using an MBraun SPS column solvent purification system. Diethyl ether, anhydrous 99% + was used as received from Sigma–Aldrich. All reactions were performed under an atmosphere of inert dinitrogen using standard Schlenk techniques unless otherwise indicated.

4.2. Preparation of [MeIn(SOOS)$_2$]$_2$ (**3**)

H_2(SOOS) (0.300 g, 1.65 mmol) in toluene (2 mL) was added drop-wise to a stirring solution of $InMe_3$ (0.263 g, 1.65 mmol) in toluene (5 mL). The solution was stirred for18 h at RT, yielding a cloudy solution and a white precipitate. The reaction mixture was filtered to remove **3** as a white powder (0.300 g, 0.967 mmol 59%). After sitting overnight at 23 °C, the reaction solution was filtered to afford block-like crystals of **3** (0.108 g, 0.348 mmol, 21%). Anal. Calc. for $C_{14}H_{30}In_2O_4S_4$: C, 27.11; H, 4.87; N, 0.00. Found: C, 27.16; H, 5.05; N, <0.3. Mp 157–158 °C. FT-IR (cm-1): 658 m, 674 m, 712 s, 809 w, 900 m, 1012 m, 1084 s, 1123 m, 1283 m, 1369 w, 1418 w, 1464 w, 2360 w, 2869 w, 2902 w, 2981 w. FT-Raman (cm^{-1}): 131 s, 181 m, 277 m, 329vs, 506 s [υ(In–C_{Me})], 660w, 675w, 1140 s, 2871w, 2903w, 2927 m. NMR data ($CDCl_3$, ppm), ^{1}H NMR: 0.00 (s, 3H, *Me*In), 2.63 (t, $^3J_{HH}$ = 5 Hz, 4H, SC*H*$_2$), 3.38–3.44 (m, 8H, C*H*$_2$OC*H*$_2$C*H*$_2$OC*H*$_2$). ^{13}C{^{1}H} NMR: −0.6 (*Me*In), 27.7 (SCH_2), 68.2 (OCH$_2$CH_2O), 72.2 (SCH$_2$CH_2O).

4.3. Preparation of [MeIn(SNNS)] (**4**)

H_2(SNNS) (0.652 g, 3.12 mmol) in thf (6 mL) was added drop-wise to a stirring solution of $InMe_3$ (0.500 g, 3.12 mmol) in thf (6 mL). The solution was stirred for 3 h at 23 °C, yielding a cloudy solution and a white precipitate. The reaction mixture was filtered to remove **4** as a colorless powder (0.824 g, 2.45 mmol 79%). The filtrate was stored at at −15 °C for 1 d and filtered to give **4** as colorless crystals (0.040 g, 0.12 mmol, 4%) Anal. Calc. for $C_9H_{21}InN_2S_2$: C, 32.15; H, 6.30; N, 8.33; S, 19.07. Found: C, 32.23; H, 6.43; N, 8.27; S, 19.09. Mp = 215–219 °C. FT-IR (cm^{-1}): 669vs, 696vs, 744w, 766 m, 884 m, 941 s, 1001w, 1021 m, 1034 m, 1077 m, 1213w, 1279w, 1300 m, 1314w, 1460 s, 2826w, 2857w, 2916w, 2956w. FT-Raman (cm^{-1}): 130 s, 158 s, 199 m, 269 m, 298 s, 335 s, 369w, 480 s [ν(In–C_{Me})], 505 s [ν_{asym}(In–C_{Me})$_2$], 670 m [ν(S–C)], 1156 m [δ(SNNS)], 1438w, 1454w, 2858w, 2921 m. NMR data ($CDCl_3$, ppm), ^{1}H NMR: 0.00 (s, 3H, *Me*In), 2.29 (s, 6H, N*Me*), 2.66–2.83 (m, 12H, MeIn(SC*H*$_2$C*H*$_2$NMeC*H*$_2$C*H*$_2$NMeC*H*$_2$C*H*$_2$S)]; ^{13}C{^{1}H} NMR: −5.3 (*Me*In), 24.2 (SCH_2), 41.9 (N*Me*), 54.7 (NCH_2CH_2N), 62.0 (SCH$_2$CH_2N).

4.4. Preparation of [MeIn(ONS_2)]$_3$ (**5**)

H_2(ONS_2) (0.611 g, 3.12 mmol) in toluene (3 mL) was added drop-wise to a stirring solution of $InMe_3$ (0.500 g, 3.12 mmol) in toluene (3 mL). The solution was stirred for 3 h at 23 °C, yielding a clear colorless solution. The reaction mixture was concentrated to 1 mL under vacuum, layered with hexanes (3 mL) and allowed to sit at 23 °C. After 7 d, the mixture was filtered to remove **5** as colorless crystals (0.786 g, 2.43 mmol 78%). Anal. Calc. for $C_8H_{18}InNOS_2$: C, 29.73; H, 5.61; N, 4.33; S, 19.84. Found: C, 29.74; H, 5.72; N, 4.26; S, 19.89. Mp = 132–136 °C. FT-IR (cm^{-1}): 591w, 669vs, 691 s, 820w, 883w, 934 m, 971 m, 998 s, 1025 m, 1077 s, 1098 m, 1112 s, 1211w, 1229 m, 1282 m, 1332w, 1351w, 1448 m, 2831w, 2880w, 2916w. FT-Raman (cm^{-1}): 126 s, 157s, 270 m, 314vs, 365w, 497vs [ν(In–C_{Me})], 670 m, 1147 m, 1441w, 2991 m, 2952 m. NMR data ($CDCl_3$, ppm), ^{1}H NMR: 0.00 (s, 3H, *Me*In), 2.50–2.62 (m, 4H, SCH_2), 2.69 (t, $^3J_{HH}$ = 5 Hz, 2H, NCH_2CH$_2$O), 2.75–2.96 (m, 4H, SCH$_2$CH_2N), 3.12 (s, 3H, O*Me*), 3.36 (t, $^3J_{HH}$ = 5 Hz, 2H, NCH$_2$CH_2O),^{13}C{^{1}H} NMR: −1.5 (*Me*In), 24.6 (SCH$_2$), 52.2 (NCH$_2$CH$_2$O), 55.3 (SCH$_2$CH_2N), 59.0 (O*Me*), 67.6 (NCH$_2$CH_2O).

4.5. Preparation of [MeIn(NNS_2)] (**6**)

H_2(NNS_2) (0.739 g, 3.12 mmol) in toluene (3 mL) was added drop-wise to a stirring solution of $InMe_3$ (0.500 g, 3.12 mmol) in toluene (3 mL). The solution was stirred for 3 h at 23 °C yielding a clear colorless solution. The reaction mixture was concentrated to 3 mL under vacuum and allowed to sit at −15 °C. After 6 d, the mixture was filtered to remove **6** as colorless crystals (0.782 g, 2.15 mmol 69%). Anal. Calc. for $C_{11}H_{25}InN_2S_2$: C, 36.27; H, 6.92; N, 7.69; S, 17.60. Found: C, 36.49; H, 7.11; N, 7.56; S, 17.59. Mp = 108–111 °C. FT-IR (cm^{-1}): 557w, 655vs, 666vs, 741 s, 788w, 885w, 935w, 953w, 997 m, 1010 s, 1058 s, 1078 s, 1093 m, 1128w, 1185w, 1271w, 1303 m, 1331w, 1389w, 1442 m, 1472 m, 2834 m, 2859w, 2913w, 2975w. FT-Raman (cm^{-1}): 139 m, 171 s, 264 m, 294 m, 328 m, 375w, 426w, 477vs [ν(In–C_{Me})], 509vw, 676w, 1134 m, 1447w, 2929 m, 2953 m. NMR data ($CDCl_3$, ppm), ^{1}H NMR: 0.00 (s, 3H, *Me*In), 1.41 (t, $^3J_{HH}$ = 7 Hz, 6H, NCH$_2$CH_3), 2.77–3.03 [m, 12H, (SCH_2CH_2)$_2$NCH_2CH_2N], 3.13 (q, $^3J_{HH}$ = 7 Hz, 4H, NCH_2CH$_3$). ^{13}C{^{1}H} NMR: −0.8 (*Me*In), 9.3 (NCH$_2$CH$_3$), 23.0 (SCH$_2$), 47.5, 47.7, 47.8 [NCH$_2$CH$_2$N(CH_2CH$_3$)$_2$], 57.4 (SCH$_2$CH$_2$).

4.6. Preparation of [MeIn(NNS_2Pr)]$_2$ (**7**)

H_2(SNNSPr) (0.329 g, 1.32 mmol) in toluene (3 mL) was added drop-wise to a stirring solution of $InMe_3$ (0.200 g, 1.25 mmol) in toluene (3 mL). The solution was stirred for 3 h at 23 °C yielding a clear colorless solution. The solvent was removed under vacuum and the resulting product was extracted with hexanes (2 × 3 mL). The mixture was filtered and the filtrate was stored at 23 °C. After 6 d, the mixture was filtered to give **7** as colorless crystals (0.098 g, 0.26 mmol 21%). Anal. Calc. for $C_{12}H_{27}InN_2S_2$: C, 38.10; H, 7.19; N, 7.41. Found: C, 37.91; H, 7.50; N, 7.37. Mp = 86–88 °C (d). FT-IR (cm^{-1}): 611 m, 668vs, 782w, 912w, 973w, 1001 m, 1022 m, 1067 s, 1086 s, 1132w, 1159w, 1196 m, 1265w, 1299 m, 1331w, 1370 m, 1448 m, 1460 m, 2797w, 2924w 2964 m. FT-Raman (cm^{-1}): 122 s, 145 s, 192 m, 260 s, 309 s, 498vs [ν(In–C_{Me})], 672 m, 1056w, 1147 m, 1453w, 2855 m, 2925 s. NMR data ($CDCl_3$, ppm), ^{1}H NMR: 0.00 (s, 3H, *Me*In), 0.81 (t, $^3J_{HH}$ = 7 Hz, 6H, NCH$_2$CH_3), 1.31–1.46 (m, 2H, NCH$_2$CH_2CH$_2$N, 2.16 [t, $^3J_{HH}$ = 7 Hz, 2H, CH_2N(CH$_2$CH$_3$)$_2$], 2.29 (q, $^3J_{HH}$ = 7 Hz, 4H, NCH_2CH$_3$), 2.39–2.60 [m, 6H, (SCH$_2$CH_2)$_2$NCH_2], 2.76–2.93 [m, 4H, SCH_2. ^{13}C{^{1}H} NMR: −1.6 (*Me*In), 11.9 (NCH$_2$CH$_3$), 20.2 (NCH$_2$CH$_2$CH$_2$N), 24.5 (SCH$_2$), 47.1 (NCH$_2$CH$_3$), 50.8 [CH$_2$N(CH$_2$CH$_3$)$_2$], 51.4 [(SCH$_2$CH$_2$)$_2$NCH$_2$], 54.6 (SCH$_2$CH$_2$N).

4.7. Preparation of [MeIn(pyrS)$_2$] (**8**)

H(pyrS) (0.328 g, 2.50 mmol) in diethyl ether (3 mL) was added drop-wise to a stirring solution of $InMe_3$ (0.200 g, 1.25 mmol) in diethyl ether (3 mL). The solution was stirred for 3 h at 23 °C, yielding a cloudy solution. The reaction mixture was filtered to remove **8** as a colorless powder (0.255 g, 0.653 mmol, 52%). The reaction filtrate was allowed to sit at 23 °C. After 6 d, the mixture

was filtered to remove **8** as colorless crystals (0.075 g, 0.19 mmol 15%). Anal. Calc. for $C_{13}H_{27}InN_2S_2$: C, 40.00; H, 6.97; N, 7.18; S, 16.43. Found: C, 39.93; H, 7.10; N, 7.12; S, 16.48. Mp = 116–117 °C. FT-IR (cm^{-1}): 577 m, 676 s, 811w, 867w, 883w, 907w, 1014 m, 1076 m, 1103 m, 1118 m, 1188w, 1225w, 1293w, 1308 m, 1348w, 1435 m, 1446 m, 1463 m, 2836 m, 2917 m, 2965 m. FT-Raman (cm^{-1}): 125 s, 160 m, 302 m, 346 s, 491vs [ν(In–C_{Me})], 676w, 906w, 1151w, 1436vw, 1462vw, 1482vw, 2845 m, 2918 m, 2967 m. NMR data ($CDCl_3$, ppm), ^{1}H NMR: 0.00 (s, 3H, *Me*In), 1.81–1.87 [m, 8H, N(CH_2CH_2)$_2$], 2.57–2.97 [m, 16H, SCH_2CH_2N(CH_2CH_2)$_2$]. ^{13}C{^{1}H} NMR: −6.2 (*Me*In), 23.5 (SCH_2), 25.2 [N(CH_2CH_2)$_2$], 54.2 (SCH_2CH_2N), 61.2 [N(CH_2CH_2)$_2$].

4.8. Polymerization experiments

0.01 mmol of the desired precatalyst (**3**, **4**, **5**, **6** or **8**), 1 μL of benzyl alcohol and 1 mmol of the desired monomer (1:1:100 indium:benzyl alcohol:monomer ratio) were added to an oven-dried ampoule charged with a magnetic stir bar and 1 mL of solvent under an inert atmosphere. The ampoule was sealed, stirred and heated to 110 °C, 85 °C, or 70 °C for the desired period of time. The ampoule was then cooled to room temperature and the resulting mixture was quenched with 3–5 drops of methanol. An aliquot was taken and solvent removed *in vacuo* for a crude sample. The rest of the mixture was then pipetted dropwise into 40 mL of cold methanol. After being stored at −35 °C for 48 h the resulting white precipitate was filtered and dried *in vacuo* to constant weight. Samples were analyzed by ^{1}H NMR spectroscopy and gel-permeation chromatography.

4.9. X-ray crystallography

Crystals of **3**–**8** were isolated from the reaction mixtures as indicated above. Single crystals were coated with Paratone-N oil, mounted using a 20 micron cryo-loop and frozen in the cold nitrogen stream of the goniometer. A hemisphere of data was collected on a Bruker AXS P4/SMART 1000 diffractometer using ω and θ scans with a scan width of 0.3° and 10 s exposure times. The detector distance was 5 cm. The data were reduced (SAINT) [37] and corrected for absorption (SADABS) [38]. The structures were solved by direct methods and refined by full-matrix least squares on F^2(SHELXTL) [39]. All non-hydrogen atoms were refined using anisotropic displacement parameters. Hydrogen atoms were included in calculated positions and refined using a riding model. Crystallographic data are given in Table 8.

Table 8
Crystallographic data for **3**, **4**, **6** and **8**.

	3	**4**	**6**	**8**
formula	$C_7H_{15}InO_2S_2$	$C_9H_{21}InN_2S_2$	$C_{11}H_{25}InN_2S_2$	$C_{13}H_{27}InN_2S_2$
fw	310.13	336.22	364.27	390.31
crystal system	triclinic	monoclinic	monoclinic	monoclinic
space group	*P*-1	*P*2(1)/c	*Cc*	*P*2(1)/c
a (Å)	8.186(1)	8.162(1)	12.049(2)	11.118(3)
b (Å)	10.841(2)	12.569(2)	10.156(2)	11.777(4)
c (Å)	14.554(3)	13.338(2)	12.907(2)	12.725(4)
α (deg)	108.625(3)	90	90	90
β (deg)	94.938(3)	102.047(2)	104.617(3)	91.753(3)
γ (deg)	110.406(2)	90	90	90
V (Å^3)	1118.4(3)	1338.1(3)	1528.4(5)	1665.3(9)
Z	4	4	4	4
F(*000*)	616	680	744	800
ρ_{calcd}, *g cm*$^{-3}$	1.842	1.669	1.583	1.557
M, *mm*$^{-1}$	2.449	2.048	1.799	1.657
T, *K*	188(1)	198(2)	173(1)	173(1)
λ, *Å*	0.71073	0.71073	0.71073	0.71073
R_1[a]	0.0206	0.0303	0.0189	0.0203
wR_2[b]	0.0555	0.0706	0.0439	0.0525

[a] $R_1 = [\Sigma||F_o|-|F_c||]/[\Sigma|F_o|]$ for $[F_o^2 > 2\sigma(F_o^2)]$.
[b] $wR_2 = \{[\Sigma w(F_o^2-F_c^2)^2]/[\Sigma w(F_o^4)]\}^{1/2}$.

4.10. Computational methods

DFT calculations were performed using Gaussian 09 at the B3LYP 6-31G* level of theory for all atoms except In, for which Stuttgart electron core pseudo-potentials (sdd) were employed [40]. All structures were geometry optimized and structural parameters for input files were derived from crystal structure data where possible. Frequency calculations were performed on all structures and gave no imaginary frequencies. Structural parameters are given in the Supplementary data.

Acknowledgments

We thank the following: Dan Durant for assistance in collecting solution NMR data; and the Natural Sciences and Engineering Research Council of Canada, the New Brunswick Innovation Foundation, the Canadian Foundation for Innovation, Mount Allison University, the Marie Curie Actions Program (FP7-PEOPLE-2013-CIG-618372) and the University of Edinburgh for financial support.

Appendix A. Supplementary data

Supplementary data related to this article can be found at http://dx.doi.org/10.1016/j.jorganchem.2016.01.020.

References

[1] C.K. Williams, Chem. Soc. Rev. 36 (2007) 1573.
[2] J. Wu, T.L. Yu, C.-T. Chen, C.-C. Lin, Coord. Chem. Rev. 250 (2006) 602.
[3] D. Garlotta, J. Polym. Environ. 9 (2001) 63.
[4] O. Dechy-Cabaret, B. Martin-Vaca, D. Bourissou, Chem. Rev. 104 (2004) 6147.
[5] Y. Cheng, S. Deng, P. Chen, R. Ruan, Front. Chem. China 4 (2009) 259.
[6] M.J. Stanford, A.P. Dove, Chem. Soc. Rev. 39 (2010) 486.
[7] See for example. (a) T. Chivers, J. Konu, Comm. Inorg. Chem. 30 (2009) 131;
(b) J. Auge, N. Lubin-Germain, J. Uziel, Synthesis (2007) 1739;
(c) S.W. Krabbe, R.S. Mohan, Top. Curr. Chem. 311 (2012) 45;
(d) Y.-C. Teo, T.-P. Loh, Org. Lett. 7 (2005) 2539;
(e) J.L. Rogers, J.J. Ernat, H. Yung, R.S. Mohan, Catal. Commun. 10 (2009) 625;
(f) U. Schneider, S. Kobayashi, Acc. Chem. Res. 45 (2012) 1331;
(g) R.K. Grasselli, J.D. Burrington, D.J. Buttrey, P. De Santo Jr., C.G. Lugmair, A.F. Volpe Jr., T. Weingand, Top. Catal. 23 (2003) 5;
(h) H.R. Kricheldorf, Chem. Rev. 109 (2009) 5579.
[8] (a) P.P. Power, Chem. Rec. 12 (2012) 238;
(b) P.P. Power, Acc. Chem. Res. 44 (2011) 627;
(c) K.S. Mandal, H.W. Roesky, Acc. Chem. Res. 45 (2012) 298;
(d) M. Asay, C. Jones, M. Driess, Chem. Rev. 111 (2011) 354;
(e) S. Yao, Y. Xiong, M. Driess, Organometallics 30 (2011) 1748;
(f) D. Martin, M. Soleilhavoup, G. Bertrand, Chem. Sci. 2 (2011) 389;
(g) P.P. Power, Nature 463 (2010) 171;
(h) T.J. Hadlington, M. Hermann, G. Frenking, C. Jones, J. Am. Chem. Soc. 136 (2014) 3028;
(i) G. Erker, D.W. Stephan, Frustrated Lewis Pairs II: Expanding the Scope, Springer, Heidelberg, 2013.
[9] G. Bouhadir, D. Bourissou, Chem. Soc. Rev. 33 (2004) 210 references therein.
[10] a) M.-H. Thibault, F.-G. Fontaine, Dalton Trans. 39 (2010) 5688;
b) M.H. Chisholm, J.C. Gallucci, K.T. Quisenberry, Z. Zhou, Inorg. Chem. 47 (2008) 2613;
c) H. Du, A.H. Velders, P.J. Dijkstra, J. Sun, Z. Zhong, X. Chen, J. Feijen, Chem. Eur. J. 15 (2009) 9836;
d) A. Arbaoui, C. Redshaw, D.L. Hughes, Chem. Commun. (2008) 4717;
e) M. Haddad, M. Laghzaoui, R. Welter, S. Dagorne, Organometallics 28 (2009) 4584;
f) S. Milione, F. Grisi, R. Centore, A. Tuzi, Organometallics 25 (2006) 266.
[11] A.P. Dove, V.C. Gibson, E.L. Marshall, A.J.P. White, D.J. Williams, Chem. Commun. (2001) 283.
[12] M.P. Blake, A.D. Schwarz, P. Mountford, Organometallics 30 (2011) 1202.
[13] a) A.F. Douglas, B.O. Patrick, P. Mehrkhodavandi, Angew. Chem. Int. Ed. 47 (2008) 2290;
b) K.M. Osten, I. Yu, I.R. Duffy, P.O. Lagaditis, J.C.-C. Yu, C.J. Wallis, P. Mehrkhodavandi, Dalton Trans. 41 (2012) 8123;
c) I. Yu, A. Acosta-Ramírez, P. Mehrkhodavandi, J. Am. Chem. Soc. 134 (2012)

12758.
[14] D.C. Aluthge, B.O. Patrick, P. Mehrkhodavandi, Chem. Commun. 49 (2013) 4295.
[15] I. Peckermann, A. Kapelski, T.P. Spaniol, J. Okuda, Inorg. Chem. 48 (2009) 5526.
[16] M. Hu, M. Wang, P. Zhang, L. Wang, F. Zhu, L. Sun, Inorg. Chem. Commun. 13 (2010) 968.
[17] J.-C. Buffet, J. Okuda, P.L. Arnold, Inorg. Chem. 49 (2010) 419.
[18] A. Pietrangelo, M.A. Hillmyer, W.B. Tolman, Chem. Commun. (2009) 2736.
[19] A. Pietrangelo, S.C. Knight, A.K. Gupta, L.J. Yao, M.A. Hillmyer, W.B. Tolman, J. Am. Chem. Soc. 132 (2010) 11649.
[20] M. Normand, E. Kirillov, T. Roisnel, J.-F. Carpentier, Organometallics 31 (2012) 1448.
[21] D.C. Aluthge, J.M. Ahn, P. Mehrkodavandi, Chem. Sci. 6 (2015) 5284.
[22] S.M. Quan, P.L. Diaconescu, Chem. Commun. 51 (2015) 9643.
[23] I.-P. Hsieh, C.-H. Huang, H.M. Lee, P.-C. Kuo, J.-H. Huang, H.-I. Lee, J.-T. Cheng, G.-H. Lee, Inorg. Chim. Acta 359 (2006) 497.
[24] C. Xu, I. Yu, P. Mehrkhodavandi, Chem. Commun. 48 (2012) 6808.
[25] L.E.N. Allan, G.G. Briand, A. Decken, J.D. Marks, M.P. Shaver, R.G. Wareham, J. Organomet. Chem. 736 (2013) 55.
[26] Crystal data for **5**: $C_{24}H_{55}In_3N_3O_{3.50}S_6$, FW 978.53, triclinic, space group *P*-1, a = 12.395(8) Å, b = 12.981(8) Å, c = 13.868(9) Å, α = 69.772(9)°, β = 72.685(9)°, γ = 63.830(8)°, V = 1851(2) Å^3, Z = 2.
[27] Crystal data for **8**: $C_{12}H_{54}In_2N_4S_4$, FW 756.62, monoclinic, space group *C*2/c, a = 34.98(3) Å, b = 15.09(1) Å, c = 13.69(1) Å, α = 90°, β = 101.80(2)°, γ = 90°, V = 7073(10) Å^3, Z = 8.
[28] A. Bondi, J. Phys. Chem. 68 (1964) 441.
[29] G.G. Briand, B.F.T. Cooper, D.B.S. MacDonald, C.D. Martin, G. Schatte, Inorg. Chem. 45 (2006) 8423.
[30] (a) S. Suh, D.M. Hoffman, Inorg. Chem. 37 (1998) 5823;
(b) T.A. Annan, R. Kumar, H.E. Mabrouk, D.G. Tuck, Polyhedron 8 (1989) 865.
[31] W. Zhao, Y. Wang, X. Liu, D. Cui, Chem. Commun. 48 (2012) 4588.
[32] Y. Hori, T. Hagiwara, Int. J. Biol. Macromol. 25 (1999) 237.
[33] Z.A.A. Hamid, A. Blencowe, B. Ozcelik, J.A. Palmer, G.W. Stevens, K.M. Abberton, W.A. Morrison, A.J. Penington, G.G. Qiao, Biomaterials 31 (2010) 6454.
[34] K.D. Karlin, S.J. Lippard, J. Am. Chem. Soc. 98 (1976) 6951.
[35] I.C. Pirmettis, M.S. Papadopoulos, S.G. Mastrostamatis, C.P. Raptopoulou, A. Terzis, E. Chiotellis, Inorg. Chem. 35 (1996) 1685.
[36] J.L. Corbin, K.F. Miller, N. Pariyadath, S. Wherland, A.E. Bruce, E.I. Stiefel, Inorg. Chim. Acta 90 (1984) 41.
[37] SAINT 7.23A, Bruker AXS, Inc, Madison, Wisconsin, USA, 2006.
[38] G.M. Sheldrick, SADABS 2008, Bruker AXS, Inc., Madison,Wisconsin, USA, 2008.
[39] G.M. Sheldrick, SHELXTL, Acta Cryst A64 (2008) 112. A64.
[40] M.J. Frisch, G.W. Trucks, H.B. Schlegel, G.E. Scuseria, M.A. Robb, J.R. Cheeseman, G. Scalmani, V. Barone, B. Mennucci, G.A. Petersson, H. Nakatsuji, M. Caricato, X. Li, H.P. Hratchian, A.F. Izmaylov, J. Bloino, G. Zheng, J.L. Sonnenberg, M. Hada, M. Ehara, K. Toyota, R. Fukuda, J. Hasegawa, M. Ishida, T. Nakajima, Y. Honda, O. Kitao, H. Nakai, T. Vreven, J.A. Montgomery Jr., J.E. Peralta, F. Ogliaro, M. Bearpark, J.J. Heyd, E. Brothers, K.N. Kudin, V.N. Staroverov, T. Keith, R. Kobayashi, J. Normand, K. Raghavachari, A. Rendell, J.C. Burant, S.S. Iyengar, J. Tomasi, M. Cossi, N. Rega, J.M. Millam, M. Klene, J.E. Knox, J.B. Cross, V. Bakken, C. Adamo, J. Jaramillo, R. Gomperts, R.E. Stratmann, O. Yazyev, A.J. Austin, R. Cammi, C. Pomelli, J.W. Ochterski, R.L. Martin, K. Morokuma, V.G. Zakrzewski, G.A. Voth, P. Salvador, J.J. Dannenberg, S. Dapprich, A.D. Daniels, O. Farkas, J.B. Foresman, J.V. Ortiz, J. Cioslowski, D.J. Fox, Gaussian 09, Revision B.01, Gaussian, Inc., Wallingford CT, 2010.